J Mater Sci (2019) 54:238–251

Chemical routes to materials

Synthesis of highly dispersed gold nanoparticles on Al_2O_3, SiO_2, and TiO_2 for the solvent-free oxidation of benzyl alcohol under low metal loadings

Jesus A. D. Gualteros[1], Marco A. S. Garcia[1], Anderson G. M. da Silva[2], Thenner S. Rodrigues[3], Eduardo G. Cândido[3], Felipe A. e Silva[3], Fabio C. Fonseca[3], Jhon Quiroz[2], Daniela C. de Oliveira[4], Susana I. Córdoba de Torresi[2], Carla V. R. de Moura[1], Pedro H. C. Camargo[2], and Edmilson M. de Moura[1,*]

[1] *Departamento de Química, Universidade Federal do Piauí, Teresina, PI 64049-550, Brazil*
[2] *Departamento de Química Fundamental, Instituto de Química, Universidade de São Paulo, São Paulo, SP 05508-000, Brazil*
[3] *Instituto de Pesquisas Energéticas e Nucleares, IPEN-CNEN, São Paulo, SP 05508-000, Brazil*
[4] *Laboratório Nacional de Luz Síncrotron, Centro Nacional de Pesquisa em Energia e Materiais, Campinas, Brazil*

Received: 23 April 2018
Accepted: 16 August 2018
Published online: 22 August 2018

ABSTRACT

We reported the organic template-free synthesis of gold (Au) nanoparticles (NPs) supported on TiO_2, SiO_2, and Al_2O_3 displaying uniform Au sizes and high dispersions over the supports. The Au-based catalysts were prepared by a deposition–precipitation method using urea as the precipitating agent. In the next step, the solvent-free oxidation of benzyl alcohol was investigated as model reaction using only 0.08–0.05 mol% of Au loadings and oxygen (O_2) as the oxidant. Very high catalytic performances (TOF up to 443,624 h^{-1}) could be achieved. Specifically, we investigated their catalytic activities, selectivity, and stabilities as well as the role of metal–support interactions over the performances. The conversion of the substrate was found to be associated with the nature of the employed support as the Au NPs presented similar sizes in all materials. A sub-stoichiometric amount of base was sufficient for the catalyst activation and the observation of the catalysts profile over the time enable insights on their recyclability performances. We believe this reported method represents a facile approach for the synthesis of uniform Au-supported catalysts displaying high performances.

Introduction

Supported gold nanoparticles (Au NPs) have attracted widespread interest in the past few decades due to their impressive properties and reactivity in several catalytic systems [1, 2]. Heterogeneous Au-based catalysts are widely employed in an extensive range of organic reactions, such as reductions [3–6], C–C couplings [7–9], and liquid- or gas-phase oxidations [10–20], being the last group focus of great current interest [21, 22]. The green oxidation of

Address correspondence to E-mail: mmoura@ufpi.edu.br

https://doi.org/10.1007/s10853-018-2827-x

organic compounds represents an eco-friendly approach since O_2 is used as the oxidizing agent. However, such reactions remain challenging due to selectivity issues and catalyst recycling [23]. The preparation or improvement in catalysts that present enhanced performance and selectivity is strongly desired since a variety of technological applications of nanotechnology rely on the possibility of controlling the NPs size, shape, composition, and structure, features that allow tailoring proprieties and boosting the activity of the catalysts [24].

Au NPs with sizes below 10 nm dispersed on metal oxides were found to be very active for oxidation reactions [25–28]. Among numerous syntheses of gold-based catalysts, two general strategies are widely used and can be highlighted targeting monodisperse Au NPs. One is the use of preformed Au NPs associated with the use of organic templates molecules (PVP, CTAB, SDS, etc.) [29–32]. The other focuses on the grafting of the oxides prior to the NPs impregnation, as the metal may interact with the organic moieties available on the support surfaces and favor the immobilization [33–35]. Although these bottom-up approaches assist the NPs synthesis and interaction with the support, the processes may be detrimental for the catalytic system since some (or all) of the active sites may be blocked, mainly when thiols groups are employed for grafting and strongly coordinating stabilizers are necessary [36]. The deposition–precipitation method with NaOH developed by Haruta et al. is an excellent technique for catalysts synthesis without the need for stabilizers or functionalization [37]. Nevertheless, this technique increases the pH of the solution, which drives a much lower deposition of metal on the support than the existing in the solution, since a substantial precipitation occurs away from the support surface [38]. Geus et al. settled a similar methodology of synthesis on which the precipitating base is urea. Such modification avoids local increase in pH and the precipitation of metal hydroxide on the solution [39].

Among many materials (e.g., polymers, activated carbon, carbon nanotubes, zeolites) used as support for Au NPs [22], metal oxides have usually been selected as function of their high stability and activity in oxidation reactions [12, 20, 40–42]; silica, titania, and alumina are among the most employed supports for this matter [22]. Owing to their different acid/base proprieties [43], studies exploring differences on catalytic activities are very promising. Although such materials seem to present similar catalytic activity for CO oxidation when chemical vapor deposition of Au was employed, suggesting no metal–support effects [44, 45], PVA-stabilized Au NPs were shown to present very distinctive performances when immobilized in different oxides (among them, commercial TiO_2, SiO_2, and Al_2O_3) for oxidative esterification of ethylene glycol [43]. Thus, systematic studies on the real support effect on oxidation reactions are the focus of great interest since it seems to be related to the catalyst synthesis and the substrate used.

Herein, we describe the synthesis of organic template-free Au-based catalysts displaying uniform sizes and high dispersion over the supports by a single step deposition/precipitation method with urea. The Au NPs were immobilized on commercial Al_2O_3, SiO_2, and TiO_2, and their catalytic activities were investigated in the solvent-free benzyl alcohol oxidation using O_2 as the oxidant, aiming at the study of support effects and metal–support interactions. Owing to Au NPs small sizes ($\sim$ 5 nm), we found that the catalysts were able to undergo the reaction with a very small amount of base for substrate activation [46–48] and low Au loadings (0.08–0.05 mol%).

Experimental

Materials and instrumentation

Analytical grade chemicals: chloroauric acid trihydrate ($HAuCl_4{\cdot}3H_2O$, 99.9%, Sigma-Aldrich), titanium(IV) oxide (TiO_2 anatase, 99.7%, Sigma-Aldrich), aluminum oxide (Al_2O_3, $\geq$ 98%, Sigma-Aldrich), silicon oxide (SiO_2, 99.5%, Sigma-Aldrich), and urea (powder, 99%, Sigma-Aldrich), were used without further purification. All solutions were prepared using deionized water (18.2 ΩM cm). The scanning electron microscopy (SEM) images were obtained using a JEOL field emission gun microscope JSM 6330F operated at 5 kV. Transmission electron microscopy (TEM) images and energy-dispersive X-ray (EDX) spectroscopy images were acquired using a FEI TECNAI G2 F20 operated at 200 kV. The Au particle size was determined used Adobe Ilustrator CS6 software, in which he particles sizes were defined by the total number of pixels and calculated from the circular areas related to the Au NPs. HRTEM analyses take into account at least 200 of

particles. Not all TEM images were presented in the paper, showing only the most representatives. The samples were prepared by drop-casting an aqueous suspension containing the catalysts over a silicon wafer, followed by drying under ambient conditions. The X-ray diffraction (XRD) data were obtained using a Rigaku-Miniflex II equipment with CuKα radiation. The diffraction pattern was measured at a 2θ range from 20° to 90° with a 1° min^{-1} step size and measuring time of 5 s *per* step. X-ray photoelectron spectroscopy (XPS) data of the samples were obtained with an SPECSLAB II (Phoibos-Hsa 3500 150, 9 channeltrons) SPECS spectrometer, with AlKα source (E = 1486.6 eV) operating at 12 kV, pass energy (E_{pass}) = 40 eV, 0.1 eV energy step and acquisition time of 1 s per point. The samples were placed on stainless steel sample-holders and were transferred under inert atmosphere to the XPS prechamber and held there for 2 h in a vacuum atmosphere. The residual pressure inside the analysis chamber was $\sim 1 \times 10^{-9}$ Torr. The binding energies (BE) of the Au 4*f* spectral peaks were referenced to the C 1*s* peak, at 284.5 eV, providing accuracy within ± 0.2 eV. Temperature-programmed reduction with hydrogen (H_2-TPR) was carried out in a Quantachrome ChemBET-Pulsar instrument equipped with a thermal conductivity detector. Typically, 0.05 g of a catalyst was dried under a He flow at 120 °C for 1 h and then cooled down to room temperature. The H_2-TPR profiles were obtained between 50 and 1100 °C in a flow of 10% H_2/N_2, with a linear temperature increasing rate of 10 °C min^{-1}. Textural characteristics of the matrices were determined from nitrogen adsorption isotherms, recorded at − 196 °C in an Autosorb IQ-Quantachrome Instrument. The samples (ca. 100 mg) were degassed for 2 h at 150 °C before analysis. Specific surface areas were determined by the Brunauer–Emmett–Teller equation (BET method) from adsorption isotherm generated in a relative pressure range $0.07 < P/Po < 0.3$. The average pore diameter was determined by the Barrett–Joyner–Halenda (BJH) method from the N_2 desorption isotherms. The CO chemisorption data and the carbon monoxide temperature-programmed desorption profiles (CO-TPD) were carried out in a Quantachrome ChemBET-Pulsar instrument equipped with a thermal conductivity detector. The area of exposed Au was measured by CO pulse chemisorption at 50 °C using a pulse of 5% CO under He environment. Prior to the chemisorption, 0.05 g of the catalyst was pretreated at 450 °C under a 10% H_2/N_2 flow, with a linear temperature increasing rate of 10 °C min^{-1}, kept at 450 °C for 1 h, and then cooled down to 50 °C. Sequentially, temperature-programmed desorption was performed by heating under a 75 cm^3 min^{-1} stream of He between 50 and 1100 °C with a heating rate of 10 °C min^{-1}. A Shimadzu GFA-EX7i flame atomic absorption spectrometer (FAAS) equipped with a pneumatic nebulizer system was used for the metal content analyses. A gold hollow cathode lamp was used throughout. The instrumental parameters and experimental conditions used for Au measurement by FAAS were: wavelength = 242.8 nm; lamp current = 5 mA; band pass = 0.7 nm; height of observation = 7 mm; air flow rate = 15 L min^{-1}; acetylene flow rate = 2.0 L min^{-1}; reading time = 5 s; nebulizer aspiration flow rate = 4 mL min^{-1}. The Au leaching analyses were performed by using a SPECTO ARCOS ICP-OES.

Synthesis of the catalysts

The described procedure was performed according to Gu et al. [49], with modifications on the order of reagents addition, urea amount, and gold precursor concentration. All the adopted adjustments are herein listed. In a typical synthesis, 1.0 g of the support (SiO_2, TiO_2, and Al_2O_3) was suspended in 100 mL of deionized water. Then, 0.7 g of urea was added and stirred for 5 min before the addition of 5 mL of 0.012 mol L^{-1} aqueous solution of $HAuCl_4$ at room temperature, under continuous stirring. The mixture was heated to 90 °C and maintained at this temperature for 4 h under stirring. After that, the solid was collected by centrifugation and washed with water (3 times, 20 mL each) and dried in an oven at 50 °C. As a final step, the material was calcined at 300 °C for 4 h in air using a ramp rate of 10 °C min^{-1}.

Catalytic experiments

The oxidation reactions were performed in a 100-mL Fischer–Porter glass reactor at 4 bar of O_2 and 100 °C, except when mentioned. In a typical reaction, the reactor was loaded with the catalyst (2.6 μmol of Au), the base (0.22 mmol of K_2CO_3), and benzyl alcohol (9.6 mmol). The temperature and stirring were maintained by a stirring plate connected to a digital controller. Usually, the reaction time was 3 h. At the

end of the reaction, the catalyst was recovered by centrifugation. The products were analyzed by gas chromatography (GC) using *p*-xylene as standard. The catalyst was used several times and washed twice with CH_2Cl_2, twice with water and calcined at 300 °C before each recycling.

Results and discussion

We stated with the synthesis of Au-based catalysts supported on different inorganic oxides (Al_2O_3, SiO_2, TiO_2). To this end, a deposition–precipitation approach was employed, in which $AuCl_4^-{}_{(aq)}$ was used as the metal precursor, urea as the precipitating/reducing agent, and water (at 90 °C) as solvent without the addition of any other stabilizing agent or organic template [39]. Figure 1 shows the SEM images for the obtained Au/Al_2O_3 (Fig. 1a, b), Au/SiO_2 (Fig. 1d, e), and Au/TiO_2 (Fig. 1g, h) catalysts. They presented similar NPs sizes, corresponding to 5.56 ± 2.08, 4.70 ± 1.39 nm, and 4.94 ± 1.37 nm, for Au/SiO_2, Au/Al_2O_3, and Au/TiO_2, respectively. Figure 1 also shows the histograms of size distribution for Au nanoparticles supported on the catalysts, indicating that our employed procedure led to the formation of supported nanoparticles displaying spherical shapes, good size distributions, and uniform Au NPs coverage onto the supports (without any detected agglomeration). To gain more insight into that matter, STEM-EDS elemental mapping images were obtained for the three catalysts, as observed in Fig. 2. Al, Si, Ti individual mappings are depicted in Fig. 2b, e, h, respectively, while the Au NPs maps of the Au/Al_2O_3, Au/SiO_2, and Au/TiO_2 catalysts are displayed in Fig. 2c, f, i, respectively.

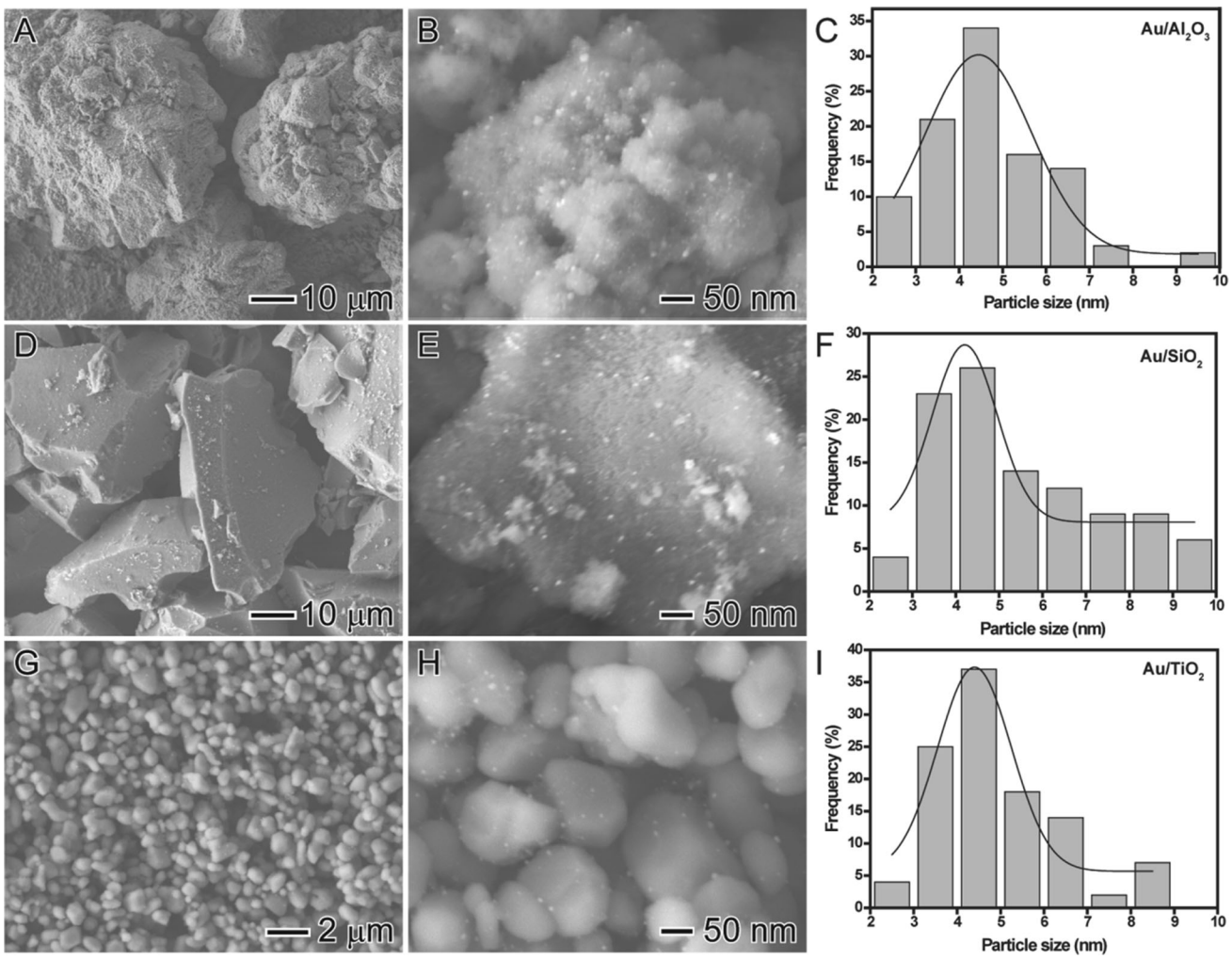

Figure 1 SEM images of Au/Al_2O_3 (**a**–**b**), Au/SiO_2 (**d**–**e**) and Au/TiO_2 (**g**–**h**) catalysts and their respective size distribution histograms.

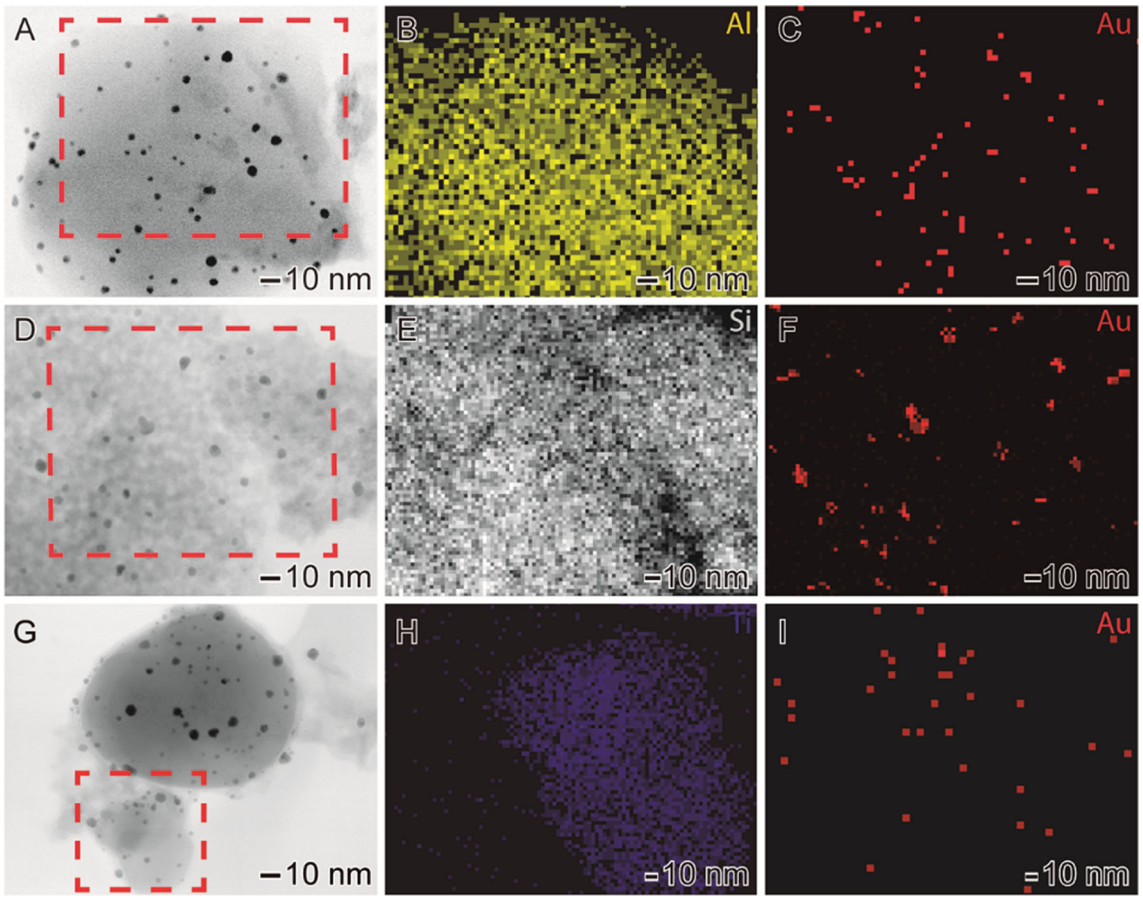

Figure 2 STEM-EDS elemental map images of Al, Si, and Ti (**b**, **e**, **h**). The maps shown in (**c**, **f**, **i**) correspond to Au/Al_2O_3, Au/SiO_2, and Au/TiO_2 catalysts, respectively.

Interestingly, just the Au/SiO_2 presented some degree of aggregation, which was not clear in the SEM images.

The Au at.% of the Au-based catalysts was determined by FAAS analyses (Table 1) and corresponded to 1.70, 1.76, and 1.72 for Au/Al_2O_3, Au/SiO_2, and Au/TiO_2, respectively. Interestingly, all catalysts presented similar Au loadings, which also were similar to the expected compositions as the $AuCl_4^-$/oxide molar ratio was kept the same for all catalysts. The corresponding number of Au sites exposed at the catalyst surface was determined by CO chemisorption (Table 1). It corresponded to 18.5, 28.8, and 44.4 μmol per gram of catalyst for Au/Al_2O_3, Au/SiO_2, and Au/TiO_2, respectively. Interestingly, despite the similar sizes and Au loading, significant differences in the number of Au surface sites were observed among the catalysts. This behavior can be associated with the magnitude of the metal–support interactions, in which metal nanoparticles interact differentially with each metal oxide. As a result, the level of adherence of a metal onto the surface of oxide

Table 1 Weight percentage, specific surface area, and number of Au active sites on the oxides obtained by FAAS, BET, and CO chemisorption analyses, respectively

Sample	Weight percentage (Au wt%)	Surface area ($m^2\ g^{-1}$)	Active sites (μmol g^{-1} of metal)	Mean pore diameter (nm)
Au/Al_2O_3	1.70	92 (111)[a]	18.5	31.5
Au/SiO_2	1.76	150 (155)[a]	28.8	56.5
Au/TiO_2	1.72	50 (51)[a]	44.4	42.5

[a]The values in parenthesis are relative to the pure commercial supports before addition of Au NPs

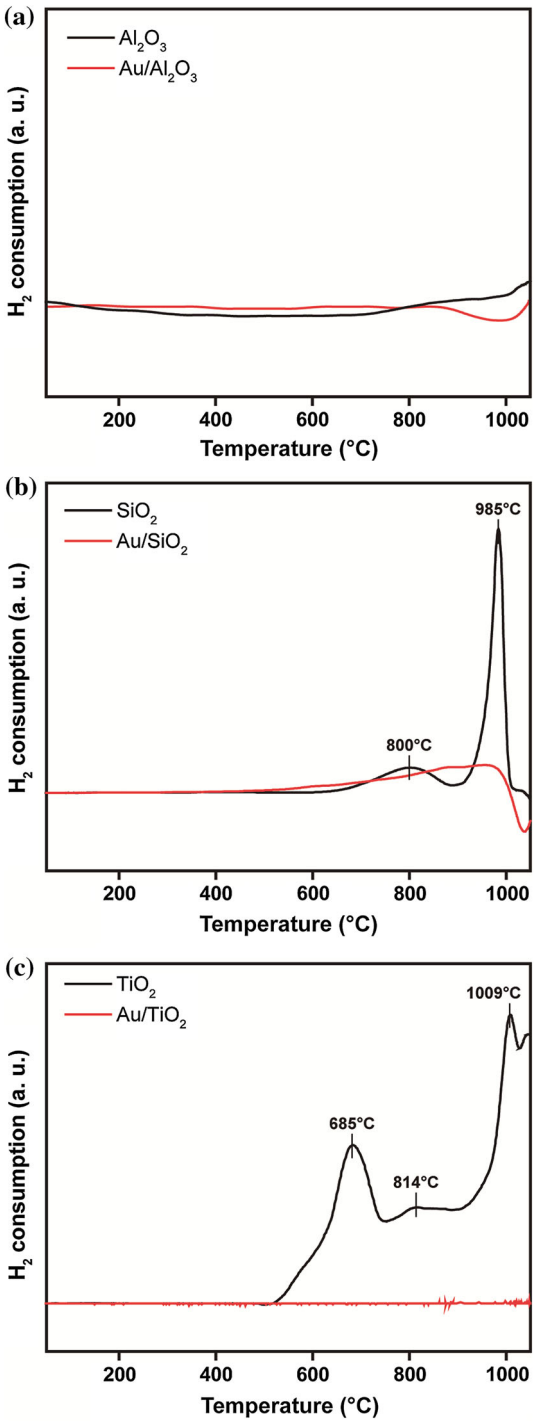

Figure 3 H_2-TPR profiles of Au catalysts and their supports: **a** Au/Al_2O_3 and Al_2O_3; **b** Au/SiO_2 and SiO_2; and **c** Au/TiO_2 and TiO_2.

structures (as a function of the degree of interaction) leads to different proportions of the nanoparticles connected to the support, and consequently, unavailable for the catalytic process [50, 51]. Specific surface areas for the materials, obtained by BET method, and their respective pore distributions (Figure S1), obtained by BHJ method, are also displayed in Table 1. All the obtained catalysts presented similar values of specific areas as compared to commercial supports prior to Au NPs deposition. The mean porosity observed follows the increasing order: $Au/Al_2O_3 < Au/TiO_2 < Au/SiO_2$.

The catalysts were also analyzed by temperature-programmed reduction (TPR) with hydrogen (H_2), as shown in Fig. 3. Among the pure commercial supports, only Al_2O_3 (Fig. 3a) showed an absence of peaks related to the H_2 consumption, indicating that no reduction processes took place in the temperature range employed in the analyzes [52–54]. On the other hand, both SiO_2 (Fig. 3b) and TiO_2 (Fig. 3c) presented peaks assigned to their reductions [43, 55, 56]. More specifically, SiO_2 presented an H_2 consumption shoulder centered at 800 °C and an intense peak of H_2 consumption centered at 985 °C. TiO_2 presented two intense peaks at 685 and 1009 °C with a shoulder at 814 °C. Interestingly, after the incorporation of Au NPs on the Al_2O_3 support, no peaks of H_2 consumption were detected, in agreement with the deposition of zero-valent Au species [43]. However, for SiO_2 and TiO_2 supports, after immobilization of Au, the signals also disappeared, suggesting an effective interaction of the nanoparticles and the support. It has been proposed that such events may be related to a suppression of hydrogen adsorption originated from the migration of the partially reduced oxides to metal surfaces due to thermal diffusion [51]. This is extremely important in catalysis due to the enhancement of catalytic activities as the consequence of effective metal–support interactions [57–61]. To shed some light on the metal oxidation, XPS analyses were performed (Fig. 4). The surface gold content and the electronic state of the catalysts were characterized, and the binding energies suggested Au(0) species for the three catalysts. Specifically, the binding energies of Au(0) $4f_{5/2}$ lines were 87.4 eV, 87.4, and 89.4 eV for Au/SiO_2, Au/TiO_2, and Au/Al_2O_3, respectively. Interestingly, the binding energies of Au(0) $4f_{7/2}$ lines were also observed for the catalysts and were the following: 83.8, 83.8, and 85.6 eV for Au/SiO_2, Au/TiO_2, and Au/Al_2O_3, respectively. Since the binding energy of the Au(0) $4f_{7/2}$ line for bulk gold is usually reported at 84.0 eV [62], the XPS analysis suggested a stronger

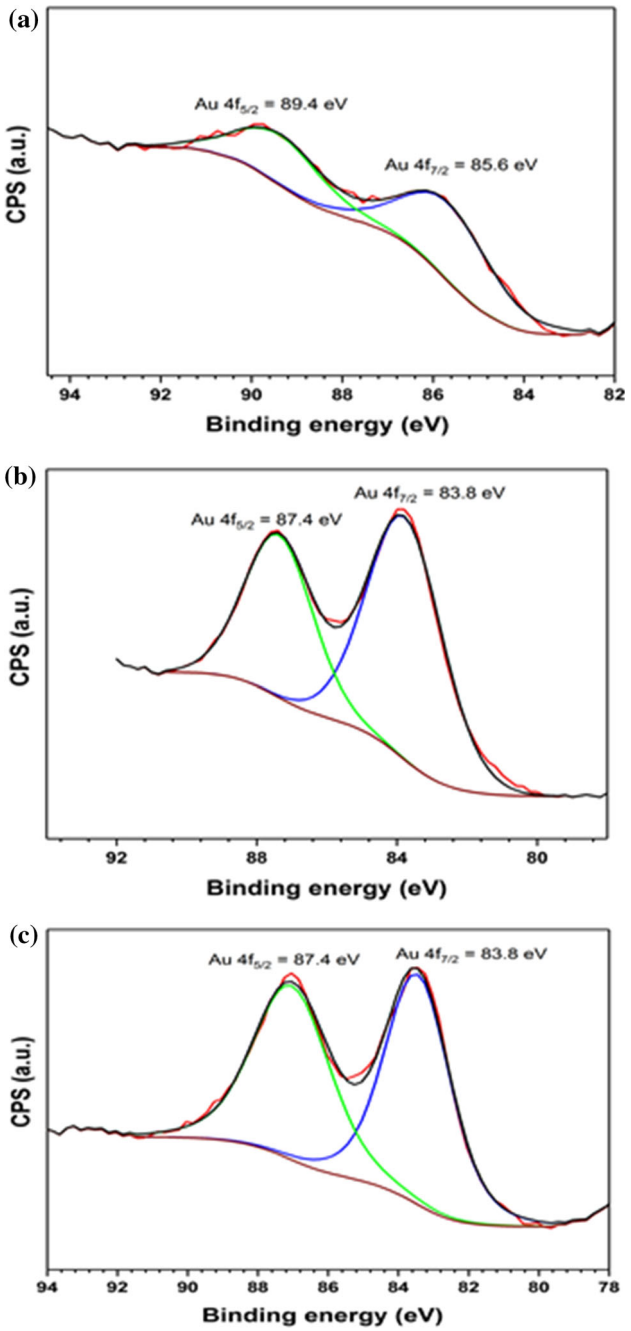

Figure 4 XPS spectra of Au 4*f* core levels for Au/Al_2O_3 (**a**), Au/SiO_2 (**b**), and Au/TiO_2 (**c**).

interaction between Au and Al_2O_3 relative to Au/TiO_2 and Au/SiO_2 samples.

Temperature-programmed desorption technique can bring some insights on the acid/base properties of the catalysts. At higher temperatures, adsorption phenomena were found to occur on stronger acid sites rather than on weaker sites when using some probe molecules, while random adsorptions occur on

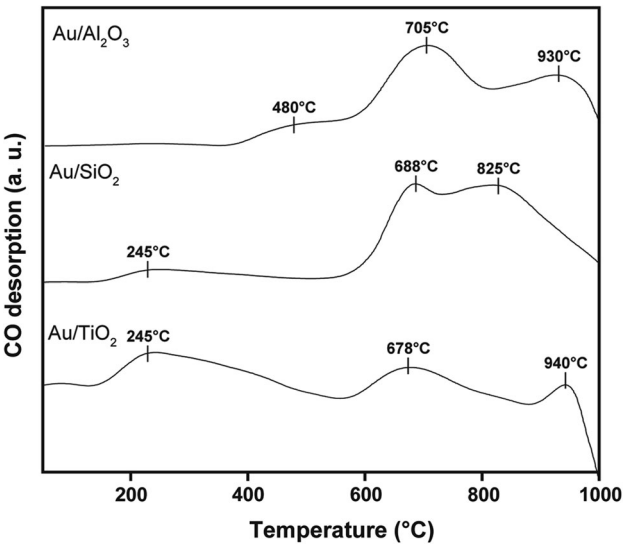

Figure 5 CO-TPD profiles of the supported Au catalysts: Au/Al_2O_3, Au/SiO_2, and Au/TiO_2.

both weak and strong sites at low temperatures [63]. Thus, temperature-programmed desorption of CO (CO-TPD) (Fig. 5) was employed in order to investigate the acidic properties of the catalysts by the temperature and intensity of CO desorption peak. This method retains its validity for hydroxylated surfaces since the CO probe molecule is a very weak Lewis base that, under the analyses conditions, provides information on the acid sites of the catalysts [64]. As observed in Fig. 5, the desorption temperature of the three samples varies considerably, indicating different interaction energies with the catalysts. The results suggest not only different structures adopted by CO on Au surfaces but also different adsorptions energies with the hydroxylated surfaces of the supports (different adsorption heatings). Although both phenomena occur simultaneously, the high affinity of CO with gold species suggests the acidity is more related to the Au NPs, with some degree of interaction with the supports. Therefore, the acidity order seemed to decrease as follows: $Au/Al_2O_3 > Au/SiO_2 > Au/TiO_2$. Interestingly, the acidity of the materials accompanied the order of acidity of their respective supports, in agreement with the effective interaction between the Au NPs and the oxide supports [43].

The obtained catalysts displayed Au NPs with well-defined shapes, uniform size distribution, and coverage of oxide supports with different degrees of acidity. These attractive features were exploited toward the solvent-free green oxidation of benzyl

alcohol under an O_2 atmosphere. In the oxidation of benzyl alcohol, the presence of an external base is considered essential for the substrate hydrogen abstraction [46–48]. Thus, K_2CO_3 was chosen considering its remarkable efficiency based on previous studies [12, 20, 65]. However, the experiments were performed using sub-stoichiometric amounts of K_2CO_3, 5 times lower than the usual amount observed in the literature to increase the attractiveness of our reported system. In order to optimize the catalytic performance of our oxidative system, a series of experiments studying the benzyl alcohol conversion and products distribution as a function of temperature and stirring speed were performed. The results of these tests are shown in Table 2 (after 3 h of reaction). As an initial screening, the catalysts were used for oxidation reactions under two temperatures. Although changing the temperature from 80 to 100 °C had no significant effect on the Au/SiO_2 performance (Entries 1 and 2), there was a remarkable influence on the activity of the Au/TiO_2 (Entries 4 and 5) and Au/Al_2O_3 catalysts (Entries 7 and 8). Also, except for the Au/SiO_2 catalyst, the temperature increasing presented an improvement toward the oxidation of the substrate to benzoic acid. It was quite unexpected that the Au/Al_2O_3 was the more active and selective catalyst at 100 °C (Entry 8), since it presents the highest acidity of the set and the lowest number of Au surface sites. However, at the same temperature, the observed activity Au/TiO_2 catalyst (Entry 5) may be explained by the highest number of superficial Au sites, even considering its lower overall surface area. The observed behavior for the Au/SiO_2 catalyst is somehow expected since it presents the highest surface area and an intermediate number of superficial Au surface sites. The same trends were not observed in 80 °C. Thus, it seems that the small amount of base used requires higher temperatures to be effective. When the stirring speed was increased from 200 to 500 rpm, significant enhancements on the activity and the selectivity of the catalysts were observed (Entries 3, 6, and 9), which can be associated with mass transfer issues overcome with the increase in the level of agitation. From these results, the temperature of 100 °C and the stirring speed of 500 rpm were chosen for further experiments.

Control experiments employing the pure commercial supports (Al_2O_3, SiO_2, and TiO_2) and without any catalyst (blank reaction) were performed (Fig. 6a). In the presence of all pure commercial supports and without a catalyst, no significant benzyl alcohol oxidation was observed even after 7 h of reaction at 100 °C. Figure 6b shows the benzyl alcohol conversion percentages as a function of time for Au/Al_2O_3 (black trace), Au/SiO_2 (blue trace), and Au/TiO_2 (red trace). It is important to note that all Au-based materials did not present pronounced induction periods since after 0.5 h all the three catalysts were able to convert the substrate. It suggests the active sites were available at the beginning, what corroborates with the TPR analyses that showed metallic Au NPs were successfully formed during the synthesis step [43]. In terms of conversion profiles as a function of time, only minor differences were observed, in which the values for conversion of

Table 2 Oxidation of benzyl alcohol catalyzed by Au/TiO_2, Au/SiO_2, and Au/Al_2O_3 catalysts in the presence of K_2CO_3 performed in non-aqueous media

Entry	Catalyst	Temperature (°C)	Conversion (%)	Selectivity (%)	
				Benzaldehyde	Benzoic acid
1	Au/SiO_2	80	36	40	60
2	Au/SiO_2	100	37	54	46
3	Au/SiO_2^a	100	56	29	71
4	Au/TiO_2	80	9	75	25
5	Au/TiO_2	100	56	59	41
6	Au/TiO_2^a	100	63	32	68
7	Au/Al_2O_3	80	13	55	45
8	Au/Al_2O_3	100	64	32	68
9	$Au/Al_2O_3^a$	100	76	22	78

Reaction conditions (solventless): benzyl alcohol (9.6 mmol), catalyst (2.6 μmol of Au), K_2CO_3 (0.22 mmol), 4 bar of O_2, 3 h, 200 rpm

[a]500 rpm

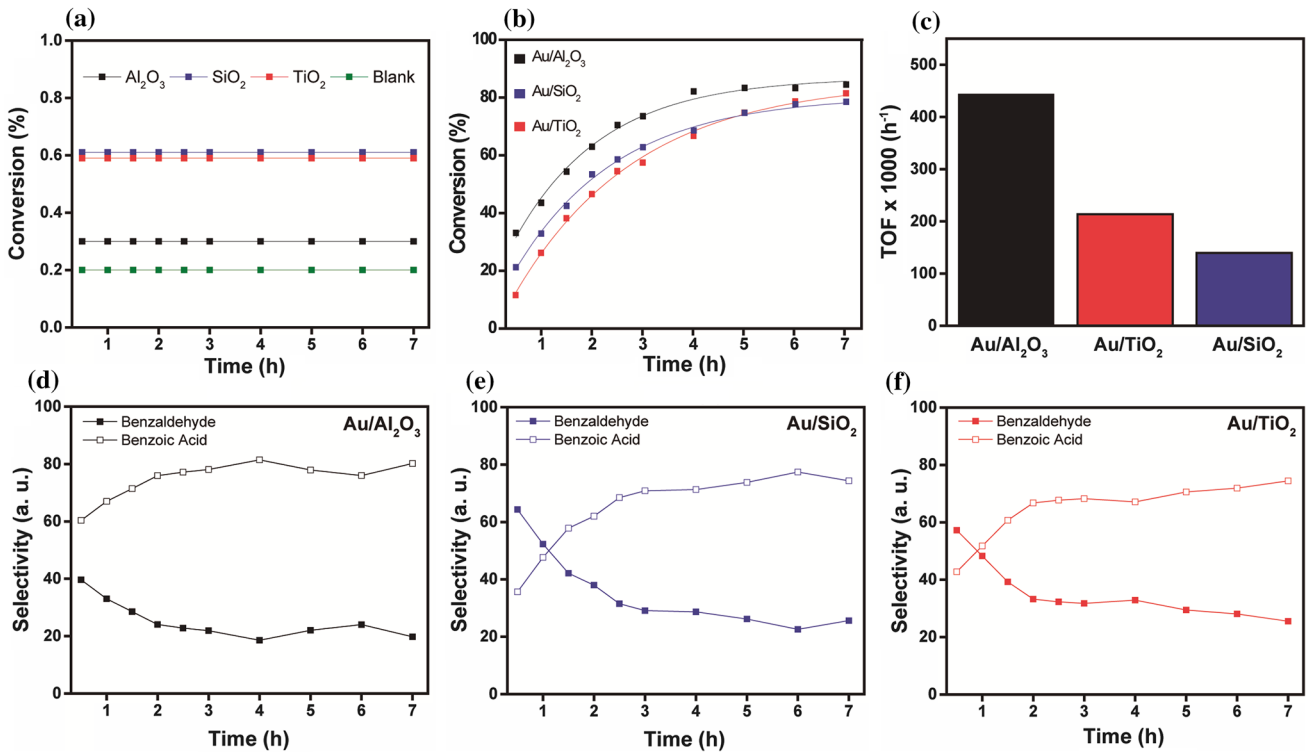

Figure 6 Conversion profiles as a function of time for **a** pure commercial supports and without any catalyst and **b** Au/Al_2O_3, Au/TiO_2, and Au/SiO_2 catalysts. **c** TOF values calculations for Au/Al_2O_3, Au/TiO_2, and Au/SiO_2 catalysts. Selectivities in the oxidation of benzyl alcohol catalyzed by **d** Au/Al_2O_3, **e** Au/SiO_2, and **f** Au/TiO_2.

benzyl alcohol during the entire reaction period did not show great variations among themselves. Here, for all catalysts, quasi-plateau profiles after 7 h of reaction were observed with the activity essentially stationary up to 24 h. The stationary activity may not be suggested as deactivation, rather it may be proposed as lack of active sites available due to strong adsorptions of the substrate/products or small quantity of base [66]. Tests with more base presented the same profile, which allow us to suggest the adsorptions are strong on the surface of the catalysts. However, when the catalytic activity is analyzed by *the turnover frequency* (TOF), considering the metallic sites, a more robust and accurate measurement of catalytic activity calculated using the CO chemisorption data, we could observe significant differences in the catalytic performances among the investigated catalysts. More specifically, Au/Al_2O_3 catalyst presented a TOF of 443,624 h^{-1} at 100 °C, which is the highest TOF observed for the set since the Au/TiO_2 and Au/SiO_2 catalysts presented TOF of 213,850 and 139,480 h^{-1}, respectively. Considering that the NPs sizes were similar in all samples (Fig. 1), the observed tendency can be associated as a combination of the contribution of the nature of the support and the number of active sites available for promoting the catalytic process. In this case, as Au/Al_2O_3 presented the lowest value of the metallic surface area (18.5 μmol g^{-1} metal). Thus, the influence of the support stood out compared to the number of surface metallic sites. The recognized acidity of Al_2O_3 may strongly contribute to the increase in the catalytic activity of Au NPs on their surface [67]. Hu et al. have previously shown that gold catalysts prepared by a PVA-stabilized approach and immobilized in commercial supports presented different activities for the oxidative esterification of ethylene glycol that are related to stronger interactions between Au and support and acidity of support. Although in such study the acidic sites were suggested to be associated with esters formation, which was not the case from the studies reported herein, the most active catalyst was the most acid as well. In addition, even with a different Au NPs synthesis methodology, the authors also observed the following descending order of activity: Au/Al_2O_3 > Au/SiO_2 > Au/TiO_2 [43]. Haruta et al. observed similar TOF values for Au/Al_2O_3, Au/SiO_2, Au/TiO_2

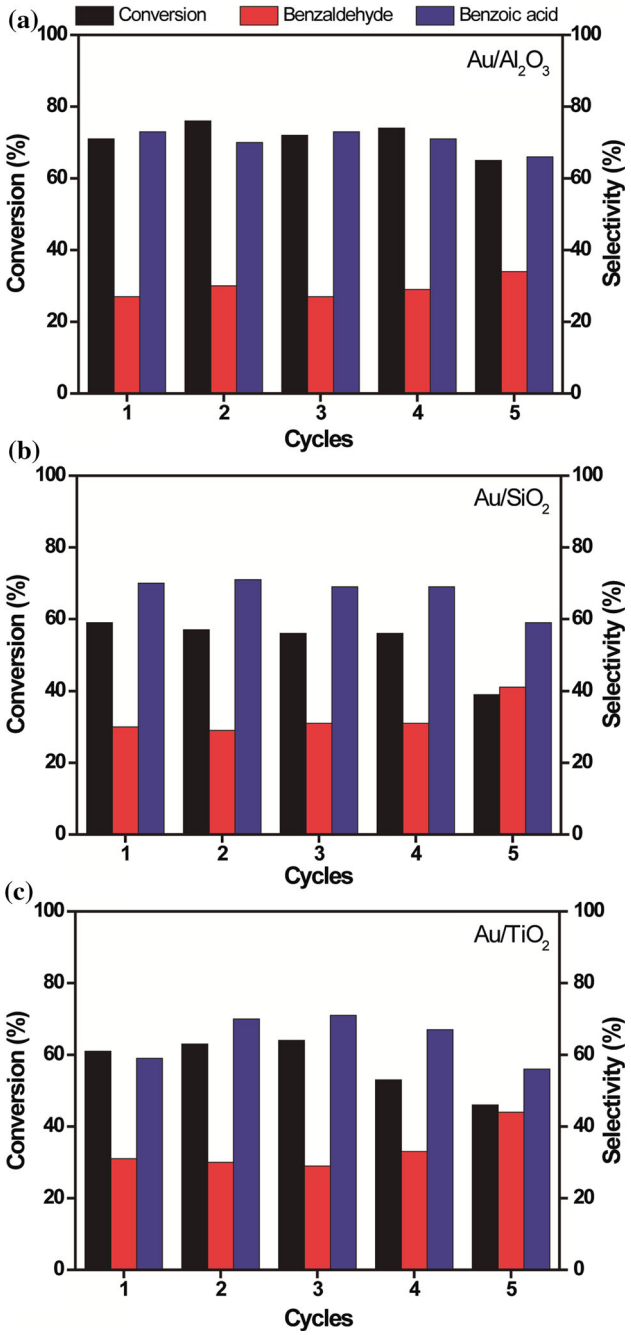

Figure 7 Recycling tests for the **a** Au/Al_2O_3, **b** Au/SiO_2, and **c** Au/TiO_2 catalysts.

for CO oxidation (when prepared by gas-phase grafting of gold acethylacetonate); however, they also associated the major controlling factor for the catalytic activity with the strong interaction of the Au NPs and the supports [68].

On the other hand, among the supports with similar levels of acidity, the effect of the number of active sites was the determinant factor in the increase in the catalytic activity, in which TiO_2 presented a higher activity comparing to SiO_2 as a function if its higher concentration of Au surface atoms (44.4 and 28.8 μmol g^{-1} metal for Au/TiO_2 and Au/SiO_2, respectively). Our results demonstrated that the Au/Al_2O_3 catalyst was the best for the proposed syntheses, which is quite unexpected according to the literature that tends to present better results using TiO_2 catalysts [43, 69–71].

All investigated catalysts could be recovered from the suspension at the end of the oxidation reaction by centrifugation and reused in the same reaction after washing with CH_2Cl_2 and water and calcination at 300 °C. As depicted in Fig. 7, all samples could be reused for five reaction cycles without great loss of activity and selectivity, indicating their good stability toward benzyl alcohol oxidation. More specifically, Au/Al_2O_3 was the most stable among the set with no significant loss of performance and selectivity after 5 cycles, followed by Au/TiO_2 with four runs of stability and Au/SiO_2, which decreased its stability after three cycles. ICP-OES analyses were performed and showed no leaching of gold was detected after 5 catalytic cycles.

Conclusions

The deposition–precipitation method with urea was used as a strategy to prepare small Au NPs which were immobilized over three commercial oxides (SiO_2, TiO_2, and Al_2O_3) without any previous modification/functionalization step and addition of any capping/stabilizing agents. The Au NPs were uniformly deposited over the entire surface of the supports, displayed spherical-like shapes, and were monodisperse in sizes. The SEM images of the NPs suggested the synthesis process were highly efficient since the sizes were reasonably similar among the three catalysts synthesized. The materials produced were successfully employed as heterogeneous catalysts toward the green oxidation of benzyl alcohol. We observed that the Au/Al_2O_3 catalyst presented a high catalytic performance (TOF = 443,624 h^{-1}) with 0.08 mol% of gold loading under optimized conditions. This behavior was associated with intrinsic acidic nature of the support, which exceeded the contribution of the number of surface sites in this sample. However, for Au/TiO_2 and Au/SiO_2 catalysts (supports with low acidities), the effect of the

number of surface sites was the determinant factor in the increase in the catalytic activity. Moreover, the catalysts presented good stabilities without significant loss of performance in 5 consecutive cycles. The data obtained suggested the support interaction with the Au NPs was the most effective feature for the observed performances. The major limitation of the catalysts was the need for thermal treatment from one run to another. Such situation was observed for the three catalysts and can be explained as a strong adsorption of the substrate/products on the catalyst surface which renders it impossible for the reaction to proceed. Our results showed that a revisit on traditional synthesis may be important for the design of novel catalysts with improved performances toward chemical transformations under green conditions.

Acknowledgements

This work was supported by FAPESP (Grant Numbers 2014/09087-4, 2014/50279-4, 15/21366-9, and 17/12407-9). F.C.F. and P.H.C.C. thank the CNPq for their research fellowships. T.S.R. and A.G.M.S. thank the FAPESP for their fellowships. E.G.C. and F.A.S. thank CNPq for their fellowships. M.A.S.G thanks CAPES for his research fellowship. J.A.D.G thanks PAEC/OEA for his fellowship.

Electronic supplementary material: The online version of this article (https://doi.org/10.1007/s10853-018-2827-x) contains supplementary material, which is available to authorized users.

References

[1] Corma A, Garcia H (2008) Supported gold nanoparticles as catalysts for organic reactions. Chem Soc Rev 37:2096–2126. https://doi.org/10.1039/b707314n

[2] Stratakis M, Garcia H (2012) Catalysis by supported gold nanoparticles: beyond aerobic oxidative processes. Chem Rev 112:4469–4506. https://doi.org/10.1021/cr3000785

[3] Luza L, Rambor CP, Gual A et al (2017) Revealing hydrogenation reaction pathways on naked gold nanoparticles. ACS Catal 7:2791–2799. https://doi.org/10.1021/acscatal.7b00391

[4] Mitsudome T, Kaneda K (2013) Gold nanoparticle catalysts for selective hydrogenations. Green Chem 15:2636–2654. https://doi.org/10.1039/c3gc41360h

[5] Bond GC (2016) Hydrogenation by gold catalysts: an unexpected discovery and a current assessment. Gold Bull 49:53–61. https://doi.org/10.1007/s13404-016-0182-8

[6] Rodrigues TS, Silva AGM, Macedo A et al (2015) Probing the catalytic activity of bimetallic versus trimetallic nanoshells. J Mater Sci 50:5620–5629. https://doi.org/10.1007/s10853-015-9114-x

[7] Li G, Jin R (2013) Catalysis by gold nanoparticles: carbon–carbon coupling reactions. Nanotechnol Rev 2:529–545. https://doi.org/10.1515/ntrev-2013-0020

[8] Milone C, Trapani M, Zanella R et al (2010) Deposition-precipitation with urea to prepare $Au/Mg(OH)_2$ catalysts: influence of the preparation conditions on metal size and load. Mater Res Bull 45:1925–1933. https://doi.org/10.1016/j.materresbull.2010.08.014

[9] Lanterna AE, Elhage A, Scaiano JC (2015) Heterogeneous photocatalytic C–C coupling: mechanism of plasmon-mediated reductive dimerization of benzyl bromides by supported gold nanoparticles. Catal Sci Technol 5:4336–4340. https://doi.org/10.1039/c5cy00655d

[10] da Silva AGM, Kisukuri CM, Rodrigues TS et al (2016) MnO2 nanowires decorated with Au ultrasmall nanoparticles for the green oxidation of silanes and hydrogen production under ultralow loadings. Appl Catal B Environ 184:35–43. https://doi.org/10.1016/j.apcatb.2015.11.023

[11] Alhumaimess M, Lin Z, Weng W et al (2012) Oxidation of benzyl alcohol by using gold nanoparticles supported on ceria foam. Chemsuschem 5:125–131. https://doi.org/10.1002/cssc.201100374

[12] Castro KPR, Garcia MAS, de Abreu WC et al (2018) Aerobic oxidation of benzyl alcohol on a strontium-based gold material: remarkable intrinsic basicity and reusable catalyst. Catalysts 8:83. https://doi.org/10.3390/catal8020083

[13] Fang W, Chen J, Zhang Q et al (2011) Hydrotalcite-supported gold catalyst for the oxidant-free dehydrogenation of benzyl alcohol: studies on support and gold size effects. Chem A Eur J 17:1247–1256. https://doi.org/10.1002/chem.201002469

[14] Oliveira AAS, Costa DS, Teixeira IF et al (2017) Red mud based gold catalysts in the oxidation of benzyl alcohol with molecular oxygen. Catal Today 289:89–95. https://doi.org/10.1016/j.cattod.2016.10.028

[15] Wang H, Shi Y, Haruta M, Huang J (2017) Aerobic oxidation of benzyl alcohol in water catalyzed by gold nanoparticles supported on imidazole containing crosslinked polymer. Appl Catal A Gen 536:27–34. https://doi.org/10.1016/j.apcata.2017.02.015

[16] Guo D, Wang Y, Zhao P et al (2016) Selective aerobic oxidation of benzyl alcohol driven by visible light on gold

nanoparticles supported on hydrotalcite modified by nickel ion. Catalysts 6:64. https://doi.org/10.3390/catal6050064

[17] Hernández WY, Aliç F, Navarro-Jaen S et al (2017) Structural and catalytic properties of Au/MgO-type catalysts prepared in aqueous or methanol phase: application in the CO oxidation reaction. J Mater Sci 52:4727–4741. https://doi.org/10.1007/s10853-016-0715-9

[18] Wu P, Bai P, Yan Z, Zhao GXS (2016) Gold nanoparticles supported on mesoporous silica: origin of high activity and role of Au NPs in selective oxidation of cyclohexane. Sci Rep 6:18817. https://doi.org/10.1038/srep18817

[19] Tanaka S, Lin J, Kaneti YV et al (2018) Gold nanoparticles supported on mesoporous iron oxide for enhanced CO oxidation reaction. Nanoscale. https://doi.org/10.1039/c7nr08895g

[20] de Abreu WC, Garcia MAS, Nicolodi S et al (2018) Magnesium surface enrichment of $CoFe_2O_4$ magnetic nanoparticles immobilized with gold: reusable catalysts for green oxidation of benzyl alcohol. RSC Adv 8:3903–3909. https://doi.org/10.1039/c7ra13590d

[21] Ballarin B, Barreca D, Boanini E et al (2017) Supported gold nanoparticles for alcohols oxidation in continuous-flow heterogeneous systems. ACS Sustain Chem Eng 5:4746–4756. https://doi.org/10.1021/acssuschemeng.7b00133

[22] Sharma AS, Kaur H, Shah D (2016) Selective oxidation of alcohols by supported gold nanoparticles: recent advances. RSC Adv 6:28688–28727. https://doi.org/10.1039/c5ra25646a

[23] Sheldon RA (2012) Fundamentals of green chemistry: efficiency in reaction design. Chem Soc Rev 41:1437–1451. https://doi.org/10.1039/c1cs15219j

[24] Camargo PHC, Rodrigues TS, Silva AGM, Wang J (2015) Metallic nanostructures. Springer, Berlin. https://doi.org/10.1007/978-3-319-11304-3

[25] Haruta M (2003) When gold is not noble: catalysis by nanoparticles. Chem Rec 3:75–87. https://doi.org/10.1002/tcr.10053

[26] Chen X, Zhu H (2011) Catalysis by supported gold nanoparticles. In: Andrews D, Scholes G, Wiederrecht G (eds) Comprehensive nanoscience and technology, vol 3. Elsevier, Amsterdam, pp 1–11

[27] Rodríguez-Reyes JCF, Friend CM, Madix RJ (2012) Origin of the selectivity in the gold-mediated oxidation of benzyl alcohol. Surf Sci 606:1129–1134. https://doi.org/10.1016/j.susc.2012.03.013

[28] Tchaplyguine M, Mikkelä MH, Zhang C et al (2015) Gold oxide nanoparticles with variable gold oxidation state. J Phys Chem C 119:8937–8943. https://doi.org/10.1021/acs.jpcc.5b00811

[29] Rossi LM, Fiorio JL, Garcia MAS, Ferraz CP (2018) Role and fate of capping ligands in colloidally prepared metal nanoparticle catalysts. Dalton Trans. https://doi.org/10.1039/c7dt04728b

[30] da Silva AGM, Rodrigues TS, Slater TJA et al (2015) Controlling size, morphology, and surface composition of AgAu nanodendrites in 15 s for improved environmental catalysis under low metal loadings. ACS Appl Mater Interfaces 7:25624–25632. https://doi.org/10.1021/acsami.5b08725

[31] Kisukuri CM, Palmeira DJ, Rodrigues TS et al (2016) Bimetallic nanoshells as platforms for metallo- and biometallo-catalytic applications. ChemCatChem 8:171–179. https://doi.org/10.1002/cctc.201500812

[32] da Silva AGM, Rodrigues TS, Haigh SJ, Camargo PHC (2017) Galvanic replacement reaction: recent developments for engineering metal nanostructures towards catalytic applications. Chem Commun 53:7135–7148. https://doi.org/10.1039/c7cc02352a

[33] Shanahan AE, Sullivan JA, McNamara M, Byrne HJ (2011) Preparation and characterization of a composite of gold nanoparticles and single-walled carbon nanotubes and its potential for heterogeneous catalysis. Xinxing Tan Cailiao/New Carbon Mater 26:347–355. https://doi.org/10.1016/s1872-5805(11)60087-5

[34] Ben Haddada M, Blanchard J, Casale S et al (2013) Optimizing the immobilization of gold nanoparticles on functionalized silicon surfaces: amine- vs thiol-terminated silane. Gold Bull 46:335–341. https://doi.org/10.1007/s13404-013-0120-y

[35] Aureau D, Varin Y, Roodenko K et al (2010) Controlled deposition of gold nanoparticles on well-defined organic monolayer grafted on silicon surfaces. J Phys Chem C 114:14180–14186. https://doi.org/10.1021/jp104183m

[36] Lopez-Sanchez JA, Dimitratos N, Hammond C et al (2011) Facile removal of stabilizer-ligands from supported gold nanoparticles. Nat Chem 3:551–556. https://doi.org/10.1038/nchem.1066

[37] Tsubota S, Haruta M, Kobayashi T et al (1991) Preparation of highly dispersed gold on titanium and magnesium oxide. Stud Surf Sci Catal 63:695–704. https://doi.org/10.1016/s0167-2991(08)64634-0

[38] Zanella R, Giorgio S, Henry CR, Louis C (2002) Alternative methods for the preparation of gold nanoparticles supported on TiO_2. J Phys Chem B 106:7634–7642. https://doi.org/10.1021/jp0144810

[39] Geus JW. Utrecht, pp 113–130

[40] de Moura EM, Garcia MAS, Gonçalves RV et al (2015) Gold nanoparticles supported on magnesium ferrite and magnesium oxide for the selective oxidation of benzyl alcohol.

RSC Adv 5:15035–15041. https://doi.org/10.1039/c4ra16159a

[41] Mirescu A, Berndt H, Martin A, Prüße U (2007) Long-term stability of a 0.45% Au/TiO_2 catalyst in the selective oxidation of glucose at optimised reaction conditions. Appl Catal A Gen 317:204–209. https://doi.org/10.1016/j.apcata.2006.10.016

[42] Abad A, Concepción P, Corma A, García H (2005) A collaborative effect between gold and a support induces the selective oxidation of alcohols. Angew Chem Int Ed 44:4066–4069. https://doi.org/10.1002/anie.200500382

[43] Ke Y-H, Qin X-X, Liu C-L et al (2014) Oxidative esterification of ethylene glycol in methanol to form methyl glycolate over supported Au catalysts. Catal Sci Technol 4:3141–3150. https://doi.org/10.1039/c4cy00556b

[44] Catalysis of gold nanoparticles deposited on metal oxides.pdf

[45] Okumura M, Tsubota S, Iwamoto M, Haruta M (1998) Chemical vapor deposition of gold nanoparticles on MCM-41 and their catalytic activities for the low-temperature oxidation of CO and of H_2. Chem Lett 27:315–316. https://doi.org/10.1246/cl.1998.315

[46] Prati L, Rossi M (1998) Gold on carbon as a new catalyst for selective liquid phase oxidation of diols. J Catal 176:552–560. https://doi.org/10.1006/jcat.1998.2078

[47] Prati L, Martra G (1999) New gold catalysts for liquid phase oxidation. Gold Bull 32:96–101. https://doi.org/10.1007/bf03216617

[48] Porta F, Prati L, Rossi M et al (2000) Metal sols as a useful tool for heterogeneous gold catalyst preparation: reinvestigation of a liquid phase oxidation. Catal Today 61:165–172. https://doi.org/10.1016/s0920-5861(00)00370-9

[49] Gu D, Tseng JC, Weidenthaler C et al (2016) Gold on different manganese oxides: ultra-low-temperature CO oxidation over colloidal gold supported on bulk-MnO_2 nanomaterials. J Am Chem Soc 138:9572–9580. https://doi.org/10.1021/jacs.6b04251

[50] Chang LY, Barnard AS, Gontard LC, Dunin-Borkowski RE (2010) Resolving the structure of active sites on platinum catalytic nanoparticles. Nano Lett 10:3073–3076. https://doi.org/10.1021/nl101642f

[51] Yoshitake H, Iwasawa Y (1992) Electronic metal support interaction in platinum catalysts under deuterium–ethene reaction conditions and the microscopic nature of the active sites. J Phys Chem 96:1329–1334. https://doi.org/10.1021/j100182a057

[52] Souza MCP, Lenzi GG, Colpini LMS et al (2011) Photocatalytic discoloration of reactive blue 5G dye in the presence of mixed oxides and with the addition of iron and silver. Braz J Chem Eng 28:393–402. https://doi.org/10.1590/s0104-66322011000300005

[53] Dimas-Rivera GL, de la Rosa JR, Lucio-Ortiz CJ et al (2014) Desorption of furfural from bimetallic Pt–Fe oxides/alumina catalysts. Materials (Basel) 7:527–541. https://doi.org/10.3390/ma7010527

[54] Oliveira RL, Bitencourt IG, Passos FB (2013) Partial oxidation of methane to syngas on Rh/Al_2O_3 and Rh/Ce-ZrO_2 catalysts. J Braz Chem Soc 24:68–75. https://doi.org/10.1590/s0103-50532013000100010

[55] Rodrigues TS, da Silva AGM, Gonçalves MC et al (2016) Catalytic properties of AgPt nanoshells as a function of size: larger outer diameters lead to improved performances. Langmuir 32:9371–9379. https://doi.org/10.1021/acs.langmuir.6b01783

[56] van Steen E, Sewell GS, Makhothe RA et al (1996) TPR study on the preparation of impregnated Co/SiO_2 catalysts. J Catal 162:220–229. https://doi.org/10.1006/jcat.1996.0279

[57] Perini L, Durante C, Favaro M et al (2015) Metal–support interaction in platinum and palladium nanoparticles loaded on nitrogen-doped mesoporous carbon for oxygen reduction reaction. ACS Appl Mater Interfaces 7:1170–1179. https://doi.org/10.1021/am506916y

[58] Lunkenbein T, Schumann J, Behrens M et al (2015) Formation of a ZnO overlayer in industrial Cu/ZnO/Al_2O_3 catalysts induced by strong metal–support interactions. Angew Chem 127:4627–4631. https://doi.org/10.1002/ange.201411581

[59] Carrasco J, López-Durán D, Liu Z et al (2015) in situ and theoretical studies for the dissociation of water on an active Ni/CeO_2 catalyst: importance of strong metal–support interactions for the cleavage of O–H bonds. Angew Chem Int Ed 54:3917–3921. https://doi.org/10.1002/anie.201410697

[60] Fang J, Li J, Zhang B et al (2015) The support effect on the size and catalytic activity of thiolated Au25 nanoclusters as precatalysts. Nanoscale 7:6325–6333. https://doi.org/10.1039/c5nr00549c

[61] da Silva AHM, Rodrigues TS, da Silva AGM et al (2017) Systematic investigation of the effect of oxygen mobility on CO oxidation over AgPt nanoshells supported on CeO_2, TiO_2 and Al_2O_3. J Mater Sci 52:13764–13778. https://doi.org/10.1007/s10853-017-1481-z

[62] Li Y, Zheng Y, Wang L, Fu Z (2017) Oxidative esterification of methacrolein to methyl methacrylate over supported gold catalysts prepared by colloid deposition. ChemCatChem 9:1960–1968. https://doi.org/10.1002/cctc.201601688

[63] Tsutsumi K, Mitani Y, Takahashi H (1983) Direct measurement of the interaction energy between solids and gases. Ix. Heats of adsorption of ammonia and pyridine on several

solids at high temperature. Bull Chem Soc Jpn 56:1912–1916

[64] Today C, Universit Z, Universit CL (1998) Surface acidity and basicity: general concepts. Catal Today 41:169–177. https://doi.org/10.1016/s0920-5861(98)00047-9

[65] Ferraz CP, Garcia MAS, Teixeira-Neto É, Rossi LM (2016) Oxidation of benzyl alcohol catalyzed by gold nanoparticles under alkaline conditions: weak vs. strong bases. RSC Adv 6:25279–25285. https://doi.org/10.1039/c6ra01795a

[66] Roduner E (2014) Understanding catalysis. Chem Soc Rev 43:8226–8239. https://doi.org/10.1039/c4cs00210e

[67] Ntho T, Aluha J, Gqogqa P et al (2013) Au/γ-Al_2O_3 catalysts for glycerol oxidation: the effect of support acidity and gold particle size. React Kinet Mech Catal 109:133–148. https://doi.org/10.1007/s11144-013-0542-9

[68] Okumura M, Tsubota S, Haruta M (2003) Preparation of supported gold catalysts by gas-phase grafting of gold acethylacetonate for low-temperature oxidation of CO and of H_2. J Mol Catal A Chem 199:73–84. https://doi.org/10.1016/s1381-1169(03)00020-7

[69] Saavedra J, Pursell CJ, Chandler BD (2018) CO oxidation kinetics over Au/TiO_2 and Au/Al_2O_3 catalysts: evidence for a common water-assisted mechanism. J Am Chem Soc. https://doi.org/10.1021/jacs.7b12758

[70] Helwani Z, Othman MR, Aziz N et al (2009) Solid heterogeneous catalysts for transesterification of triglycerides with methanol: a review. Appl Catal A Gen 363:1–10. https://doi.org/10.1016/j.apcata.2009.05.021

[71] Yang K, Meng C, Lin L et al (2016) A heterostructured TiO_2–C_3N_4 support for gold catalysts: a superior preferential oxidation of CO in the presence of H_2 under visible light irradiation and without visible light irradiation. Catal Sci Technol 6:829–839. https://doi.org/10.1039/c5cy01009h